Journal of Computational Physics **151,** 458–478 (1999)
Article ID jcph.1999.6193, available online at http://www.idealibrary.com on IDEAL®

Two-Dimensional Vlasov Simulation of Raman Scattering and Plasma Beatwave Acceleration on Parallel Computers

M. L. Bégué, A. Ghizzo, and P. Bertrand

Laboratoire de Physique des Milieux Ionisés, Université Henri Poincaré Nancy-I, P.O. Box 239, 54506 Vandoeuvre les Nancy Cedex, France
E-mail: ghizzo@lpmi.u-nancy.fr

Received June 10, 1998; revised December 22, 1998

A two-dimensional relativistic Vlasov model for a multi-computer environment was developed to address the particle acceleration process in phase space, including situations relevant to forward Raman scattering (FRS) and plasma beatwave acceleration (PBWA). Attention was focused on its accuracy, stability, efficiency properties, and implementation facilities on massively parallel computers. The two-dimensional Vlasov code has been adapted to optimally use the particular parallel architecture of the T3D or T3E computer (both processor's specifications and node-to-node communications). Results obtained on a 64-node Cray T3D clearly show the details of particle acceleration in phase space, including very low density regions where particles-in-cell (PIC) codes simply run out of calculation particles. On the other hand optimization obtained on the T3D architecture leads to a CPU time of 9.5 μs per time step, per particle, per processor indicating that one processor on the Cray C94 computer is equivalent to 20 processors on the T3D computer. Finally, we note that the Vlasov code is able to achieve high parallel efficiency with scalability of order 2.

Key Words: laser-plasma interaction; parallelism on T3E; semi-Lagrangian Vlasov codes.

1. INTRODUCTION

Since the suggestion by Tajima and Dawson [1] of particle acceleration by means of plasma waves in 1979, various schemes have been proposed to excite large amplitude electron plasma waves (EPW) (theoretically capable of reaching an electric field of the order of GV/m). Such a wave is of interest as a particle accelerator concept since electron plasma wave amplitude can largely exceed the breaking limit of the standard metallic cavity based accelerator, which is of the order of 30 MV/m. One of the promising schemes for exciting

0021-9991/99 $30.00

strong plasma waves remains the plasma beatwave accelerator (PBWA), which is based on the injection of two electromagnetic waves in a plasma of low density. The difference of frequencies of the two electromagnetic waves is chosen to be equal to the plasma frequency. In these conditions, the beat of theses two waves resonantly induces a high-phase velocity longitudinal plasma wave which traps and accelerates electrons to ultra relativistic energies. Because the excitation of the plasma wave relies on the resonant temporel beating of lasers, the pulse durations have to be much greater than the plasma period ω_p and precise matching is crucial. A very similar mechanism is involved in the forward Raman scattering (FRS) process, in which an incident electromagnetic wave decays into an electron plasma wave and a scattered electromagnetic wave.

In previous papers, examples of PBWA and FRS simulations using one-dimensional Vlasov simulations with periodic or open-system boundary conditions have been carried out (see [2–4]). Such codes render possible a detailed examination of the low density regions of the phase space especially the description of the tail phenomena, where only a small number of electrons is involved. In this type of problem, "particles-in-cell" (PIC) codes suffer from poor statistics. This is because the PIC codes lack enough simulation particles to display the detailed phase space structures of the distribution function which is often obtained in those regions of phase space where particle and phase velocities are comparable and where trapping or plasma wavebreaking occurs. A second advantage is the noiseless character of the Vlasov code. Thus during the simulation, we can analyze the microscopic wave-particle dynamics, the tail formation, and the energy transfer from the pump and idler waves to electrons.

A primary motivation for the present work is to take into account two-dimensional spatial effects in the particle acceleration. The nature of the computational algorithm (with the eulerian characterization of the distribution function) along with the large memory requirements of the phase space representation (i.e., with at least four phase space variables to describe the electron distribution function) makes this problem a good candidate for parallel execution. Hence a secondary goal of this work is to address key issues involved in parallelizing a Vlasov code in an electromagnetic relativistic regime.

The paper is organized as follows. In Section 2 the plasma geometry is described and the governing equations are derived. The numerical algorithm implemented on the parallel Cray T3D computer is presented in Section 3, including details on the time splitting scheme used for integrating the Vlasov equation and the transposition method of distribution function used here. Issues related to parallelizing the code are then adressed in this section. Numerical results relevant to FRS are then presented in Section 4 and comparisons are made with the one-dimensional case in order to test the validity of the Vlasov code. This section also includes a discussion on the Manley–Rowe partition and the influence of the transverse gaussian pump profile on the particle acceleration mechanism. A more complex situation is then described in Section 5 relevant to plasma beatwave acceleration including Stokes and anti-Sokes cascades and side-scattering. Concurrent performance of the model is discussed in Section 6. Conclusions and future work are offered in Section 7.

2. THE 2D RELATIVISTIC VLASOV MODEL

In forward Raman scattering (FRS) and plasma beatwave acceleration (PBWA), the ponderomotive force drives a large amplitude plasma wave along the laser wavevector direction and produces trapped electrons with very high momenta. To model this, we consider an

infinite homogeneous plasma of density n_o in both the x and y direction with a laser wavevector in the x direction: all field quantities being a function of the space variables x and y. Using the Coulomb gauge $\nabla \cdot \mathbf{A} = 0$, we restrict the potential vector $\mathbf{A}$ to be in the z direction only (linear polarization). Recalling that

$$\mathbf{E} = -\nabla\Phi - \frac{\partial \mathbf{A}}{\partial t} \tag{1}$$

we have in the perpendicular direction z,

$$E_z = -\frac{\partial A_z}{\partial t} \tag{2}$$

and in the plasma plane,

$$E_x = -\frac{\partial \Phi}{\partial x} \qquad \text{and} \qquad E_y = -\frac{\partial \Phi}{\partial y}. \tag{3}$$

The electron distribution function $F(x, y, \mathbf{p}, t)$ obeys the relativistic Vlasov equation

$$\frac{\partial F}{\partial t} + \frac{\mathbf{p}}{m\gamma}\frac{\partial F}{\partial \mathbf{r}} + e\left[\mathbf{E} + \frac{\mathbf{p}}{m\gamma} \times \mathbf{B}\right]\frac{\partial F}{\partial \mathbf{p}} = 0, \tag{4}$$

where $\mathbf{r} = (x, y, 0)$ and $\mathbf{p} = (p_x, p_y, p_z)$ with the Lorentz factor given by

$$\gamma = \sqrt{1 + \left(\frac{\mathbf{p}^2}{m^2c^2}\right)}. \tag{5}$$

But huge memory requirements are necessary to handle a full 2D1/2 model, i.e., five phase space variables x, y, p_x, p_y, and p_z as discussed above. Thus let us consider the following class of exact solutions of (4),

$$F(x, y, p_x, p_y, p_z, t) = f(x, y, p_x, p_y, t)\delta[p_z - P_z(x, y, t)] \tag{6}$$

which is relevant to low perpendicular temperature plasma. The reduced 2D distribution function $f(x, y, p_x, p_y, t)$ describing the particle motion in the (x, y) plane satisfies the two-dimensional relativistic Vlasov equation

$$\frac{\partial f}{\partial t} + \frac{p_x}{m\gamma}\frac{\partial f}{\partial x} + \frac{p_y}{m\gamma}\frac{\partial f}{\partial y} + e\left[E_x - \frac{P_z B_y}{m\gamma}\right]\frac{\partial f}{\partial p_x} + e\left[E_y + \frac{P_z B_x}{m\gamma}\right]\frac{\partial f}{\partial p_y} = 0 \tag{7}$$

with a Lorentz factor of the form

$$\gamma = \sqrt{1 + \frac{p_x^2 + p_y^2 + P_z^2(x, y, t)}{m^2c^2}}. \tag{8}$$

Assuming the relativistic contribution is due to accelerated particles only along the longitudinal direction (i.e., laser propagation direction or x direction), the Lorentz factor can be simplified to $\gamma \simeq \sqrt{1 + p_x^2/m^2c^2}$. This is valid for moderate intensity with quiver momentum of order 0.1 mc. Furthermore since the relative number of accelerated particles in the x direction remains very small in the beatwave experiment, we can taken $\gamma \simeq 1$, in the term $e[E_x - P_z B_y/m\gamma]\partial f/\partial p_x$ since $\partial f/\partial p_x \ll n_0/m^3c^3$, for a small population of accelerated

particle density, which remains small in comparison with the mean electron density n_0 (the normalized quantity is then $\partial \hat{f}/\partial \hat{p}_x \ll 1$ where the dimensionless space and momentum variables used in simulation have been taken to be $\hat{x} = x\omega_p/c$ and $\hat{p}_x = p_x/mc$. The time $\hat{t}$ and the distribution function $\hat{f}$ are then normalized to the inverse plasma frequency ω_p^{-1} and to n_0/m^2c^2; the electron density in then normalized to n_0. Comparison with a full relativistic Vlasov code does not give a difference for the range of laser intensities considered here.

In this model, the transverse momentum effects in the z direction are described by a cold "fluid" model. The transverse momentum $P_z(x, y, t)$ is simply obtained through the conservation of the canonical generalized momentum $P_z + eA_z = 0$. Deriving with respect to time and using (2) yield

$$\frac{\partial P_z}{\partial t} = eE_z. \tag{9}$$

The plasma self consistent electric field components E_x and E_y are given by Eqs. (3) while the potential Φ obeys the Poisson equation

$$\Delta\Phi = -\frac{e}{\varepsilon_o}[n_e(x, y, t) - n_o]. \tag{10}$$

n_o is the homogeneous ion density and $n_e = \int f\, dp_x\, dp_y$. The electromagnetic field components (E_z, B_x, B_y) obey Maxwell's equations

$$\frac{\partial B_x}{\partial t} = -\frac{\partial E_z}{\partial y} \tag{11}$$

$$\frac{\partial B_y}{\partial t} = -\frac{\partial E_z}{\partial x} \tag{12}$$

$$\frac{\partial E_z}{\partial t} = c^2\left(\frac{\partial B_y}{\partial x} - \frac{\partial B_x}{\partial y}\right) - \frac{J_z}{\varepsilon_o}, \tag{13}$$

where $J_z = en_eP_z/m$.

3. THE NUMERICAL PARALLEL ALGORITHM

3.1. *Semi-Lagrangian Advection*

In an Eulerian advection scheme an observer watches the world evolve around him at a fixed geographical point. Such schemes work well on regular cartesian meshes (facilitating vectorisation and parallelization of the resulting code), but often lead to overly restrictive time steps due to considerations of computational stability. In a Lagrangian advection scheme (as PIC codes) an observer watches now the world evolve around him as he travels with the fluid particle. Such schemes can often use much larger time steps than Eulerian ones, but have the disadvantage that an initially regularly spaced set of particles will generally evolve to a highly irregularly spaced set at later times. The idea behind semi-Lagrangian advection (see [6]) is to try to get the best of both worlds: the regular resolution of Eulerian schemes and the enhanced stability of Lagrangian ones. This is achieved by using a different set of particles at each time step, the set of particles being chosen such that they arrive exactly at the points of a regular cartesian mesh at the end of the time step.

The semi-Lagrangian Vlasov code (see Refs. [2, 3]) has been adapted to optimally use the particular parallel architecture of the Cray T3D and then T3E. For example, in the case of a one-dimensional electrostatic problem described by a Vlasov equation of type $\frac{\partial f}{\partial t} + v\frac{\partial f}{\partial x} + \frac{eE}{m}\frac{\partial f}{\partial v} = 0$, the well-known fractional step or "splitting scheme" (see Refs. [7, 8] for bidimensional models) used to integrate the distribution function $f(x, v, t)$ (in which we shift the distribution function alternatively in the x direction leading to the mathematical form $f^*(x, v) = f(x - v\Delta t, v)$ and then in the v direction with the corresponding expression $f^{**}(x, v) = f^*(x, v - eE\Delta t/m)$) is straightforward to parallelize. Each shift is easily parallelized by just assigning a fraction of the distribution function to each node (for example, for the shift in the x direction, we break the v direction into regions with a region assigned to a node), and thus each processor handles those grid points in its region. Then a transposition of the distribution function is required to perform the parallelized shift in the second direction.

3.2. *Two-Dimensional Relativistic Vlasov Equation*

Let us define $f^n(\tilde{x}, y, p_x, p_y) = f(\tilde{x}, y, p_x, p_y, t_n = n\Delta t)$ as the function distributed among the processors along the x direction and $f^n(x, y, \tilde{p}_x, p_y)$ as the function obtained by transposition, i.e., with a decomposition domain in the p_x direction. The Vlasov equation is then advanced using the time splitting scheme, which involved here four steps:

Step A1. Transpose the function and shift in the x and y direction,

$$\begin{aligned} f^n(\tilde{x}, y, p_x, p_y) &\Rightarrow f^n(x, y, \tilde{p}_x, p_y) \\ f^*(x, y, \tilde{p}_x, p_y) &= f^n\left(x - \frac{\tilde{p}_x}{m\gamma}\frac{\Delta t}{2}, y, \tilde{p}_x, p_y\right) \\ f^{2*}(x, y, \tilde{p}_x, p_y) &= f^*\left(x, y - \frac{p_y}{m\gamma}\frac{\Delta t}{2}, \tilde{p}_x, p_y\right). \end{aligned} \tag{14}$$

and then make the inverse transposition, $f^{2*}(x, y, \tilde{p}_x, p_y) \Rightarrow f^{2*}(\tilde{x}, y, p_x, p_y)$.

Step A2. Compute the electromagnetic field and fluid momentum P_z at time $t_{n+1/2}$ and then shift in $\mathbf{p}$ space for a time step Δt,

$$\begin{aligned} f^{3*}(\tilde{x}, y, p_x, p_y) &= f^{2*}\left(\tilde{x}, y, p_x - e\left(E_x - \frac{P_z B_y}{m}\right)\Delta t, p_y\right) \\ f^{4*}(\tilde{x}, y, p_x, p_y) &= f^{3*}\left(\tilde{x}, y, p_x, p_y - e\left(E_y + \frac{P_z B_x}{m\gamma}\right)\Delta t\right). \end{aligned} \tag{15}$$

Step A3. Between $t_{n+1/2}$ and t_{n+1}, we repeat again Step A1. Cubic spline interpolation is then used to obtain the distribution function at the grid point at each integration step. The equation for the perpendicular motion (9) is solved between $t_{n-1/2}$ and $t_{n+1/2}$ using the time centered scheme,

$$P_{z\,i+\frac{1}{2},j+\frac{1}{2}}^{n+\frac{1}{2}} = P_{z\,i+\frac{1}{2},j+\frac{1}{2}}^{n-\frac{1}{2}} + e\Delta t E_{z\,i+\frac{1}{2},j+\frac{1}{2}}^{n}. \tag{16}$$

Poisson equation (10) is solved at time $t_{n+1/2}$ using a parallel FFT[1] program implemented on the Cray T3E computer.

[1] FFT, *f*ast *F*ourier *t*ransform.

3.3. *Maxwell Equations*

The Maxwell equations (11), (12), and (13) are solved using a usual leapfrog scheme leading to

$$\begin{aligned} B^{n+\frac{1}{2}}_{x\ i+\frac{1}{2},j} &= B^{n-\frac{1}{2}}_{x\ i+\frac{1}{2},j} - \frac{\Delta t}{\Delta y}\left(E^{n}_{z\ i+\frac{1}{2},j+\frac{1}{2}} - E^{n}_{z\ i+\frac{1}{2},j-\frac{1}{2}}\right) \\ B^{n+\frac{1}{2}}_{y\ i,j+\frac{1}{2}} &= B^{n-\frac{1}{2}}_{y\ i,j+\frac{1}{2}} + \frac{\Delta t}{\Delta x}\left(E^{n}_{z\ i+\frac{1}{2},j+\frac{1}{2}} - E^{n}_{z\ i-\frac{1}{2},j+\frac{1}{2}}\right) \end{aligned} \tag{17}$$

$$\begin{aligned} E^{n+1}_{z\ i+\frac{1}{2},j+\frac{1}{2}} = E^{n}_{z\ i+\frac{1}{2},j+\frac{1}{2}} &- \frac{\Delta t}{\varepsilon_o} J^{n+\frac{1}{2}}_{z\ i+\frac{1}{2},j+\frac{1}{2}} + \frac{c^2\Delta t}{\Delta x}\left(B^{n+\frac{1}{2}}_{y\ i+1,j+\frac{1}{2}} - B^{n+\frac{1}{2}}_{y\ i,j+\frac{1}{2}}\right) \\ &- \frac{c^2\Delta t}{\Delta y}\left(B^{n+\frac{1}{2}}_{x\ i+\frac{1}{2},j+1} - B^{n+\frac{1}{2}}_{x\ i+\frac{1}{2},j}\right). \end{aligned} \tag{18}$$

Notice that the solution of (18) involves the knowledge of the current density $J_z^{n+1/2}$ at the middle of the time interval $t_{n+1/2}$ which is approximated by

$$J^{n+\frac{1}{2}}_{z\ i+\frac{1}{2},j+\frac{1}{2}} = \frac{e}{2m} P^{n+\frac{1}{2}}_{z\ i+\frac{1}{2},j+\frac{1}{2}}\left[n^{n}_{e\ i+\frac{1}{2},j+\frac{1}{2}} + n^{n+1}_{e\ i+\frac{1}{2},j+\frac{1}{2}}\right]. \tag{19}$$

4. FORWARD RAMAN SCATTERING PROBLEM

4.1. *Homogeneous Pump Laser Profile*

The FRS instability is a parametric instability involving three waves: the incident electromagnetic wave, here referred to as the "pump" wave (ω_o, k_o) which drives two unstable waves; a scattered electromagnetic wave (ω_s, k_s); and an electron plasma wave (ω_e, k_e). The Raman instability occurs when the usual matching conditions hold:

$$\omega_o(k_o) + \Delta\omega = \omega_s(k_s) + \omega_e(k_e) \qquad \text{and} \qquad k_o = k_s + k_e. \tag{20}$$

We assume perfect k-matching (since we have a periodic simulation and mode numbers match exactly), while $\Delta\omega$ contains the mismatch (if any). The matching conditions can be satisfied only if $n_e \le n_{crit}/4$ where n_{crit} is the critical density above which the electromagnetic wave will not propagate. (A high amplitude electromagnetic wave can however propagate through an overdense plasma provided that the electron quiver velocity is close to the velocity of light.) In order to compare our simulation with analytical predictions, it is convenient, for such a Raman problem, to introduce the classic three-oscillator model. Defining the complex action amplitude $a_{o,s,e}$ (such that the action density is given by $S = aa^*$), the oscillator model in a lossless medium is given by

$$\begin{aligned} \left(\frac{\partial}{\partial t} + v_{go}\frac{\partial}{\partial x}\right)a_o &= -Ca_s a_e \\ \left(\frac{\partial}{\partial t} + v_{gs}\frac{\partial}{\partial x}\right)a_s &= Ca_s a_e^* \\ \left(\frac{\partial}{\partial t} + v_{ge}\frac{\partial}{\partial x}\right)a_e &= Ca_o a_s^*. \end{aligned} \tag{21}$$

Here we have defined $C = k_e/2\sqrt{2\omega_o\omega_e\omega_s}$. The plasma is considered unmagnetized. In the three-oscillator model with periodic boundary conditions (see Ref. [3]), we can drop the group-velocity-times spatial gradient terms, and convert to ordinary coupled differential equations and analyze action density conservation. Equations (21) yield the Manley–Rowe partition,

$$C_s(t) = a_o a^*_{o,k_x=k_o,k_y=0} + a_s a^*_{s,k_x=k_s,k_y=0} = C_s(0) = \text{const} \tag{22}$$

which means photon conservation and

$$C_e(t) = a_o a^*_{o,k_x=k_o,k_y=0} + a_e a^*_{e,k_x=k_e,k_y=0} = C_e(0) - 2\Gamma \int_0^t |a_e|^2\, dt. \tag{23}$$

If losses are taken equal to zero, Eq. (23) means that when one pump photon disappears, one plasmon is created. Indeed the action sum C_e generally decreases since it involves a plasma wave which can accelerate and trap particles and thus loses energy and action. Thus the utility of a periodic simulation (the transverse direction y being homogeneous in both the plasma system and electromagnetic field spatial structures) is clearly demonstrated since it allows one to use action conservation to separate the effects of three-wave interaction from those due to nonlinear wave-particle interaction. We have performed numerical simulations using periodic boundary conditions in both the x and y directions and an initial state consisting of a significant electromagnetic pump propagating in the x positive direction and homogeneous in the y direction and a propagating electrostatic plasma wave of modest amplitude, acting as a perturbation from which FRS can grow, since a Vlasov code is essentially noiseless. Since the velocities are normalized to c, and frequencies to ω_p, the choice of $k_o (= 2k_s \text{ or } 2k_e)$ determines the plasma box length L_x in terms of c/ω_p. The plasma was chosen with two electron temperature components, the majority (95%) component with a 15 keV temperature in both directions p_x and p_y (high enough for electron Landau damping to subdue the usually rapidly growing but here unwanted backward stimulated Raman scattering) and a minority (5%) p_x-component at 100 keV (to enhance wave-particle interaction). With these parameters, a good frequency match was obtained by choosing $k_o c/\omega_p = 2.4$, i.e., a box length $L_x = 5.23c/\omega_p$ (we take in the second direction $L_y = 20c/\omega_p$). The normalized pump electric field amplitude is $eE_o/m\omega_p c = 0.28$ which gives a quiver momentum of $p_{osc}/mc \simeq 0.10$ (for a $10.6\,\mu\text{m} - CO_2$ laser, the corresponding intensity is $1.8\,10^{14}$ W/cm^2). The density as compared tothe critical density is then $n_e/n_{crit} \simeq 0.15$.

The time behavior of the action densities from the 2D Vlasov simulation are shown in Figs. 1 and 2 together with the relevant action sum. The action is transferred back and forth between the pump and daughter waves in a classic fashion previously met in a 1D Vlasov simulation (see Ref. [3]) with an accumulating loss due the plasma wave and the action transfer to accelerated particles. As expected from (22) the action sum C_s for the electromagnetic wave pair is well conserved (to within 2%), while the pump-plus-plasma sum C_e decreases. Figure 3 shows the $x - p_x$ phase space representation $f\ (x, y = L_y/2,\ p_x,\ p_y = 0)$ afforded by the Vlasov code. Here color shading is used to indicate the relative values of normalized phase space density between 10^{-3} and 10^{-4}. Figure 3 is in good agreement with numerical results obtained directly by a 1D periodic Vlasov code and seems to indicate a classic acceleration process when the transverse laser profile is chosen to be homogeneous: they clearly exhibit the acceleration of positive velocity particles followed by the trapping and formation of vortices with spiral orbits in the phase space.

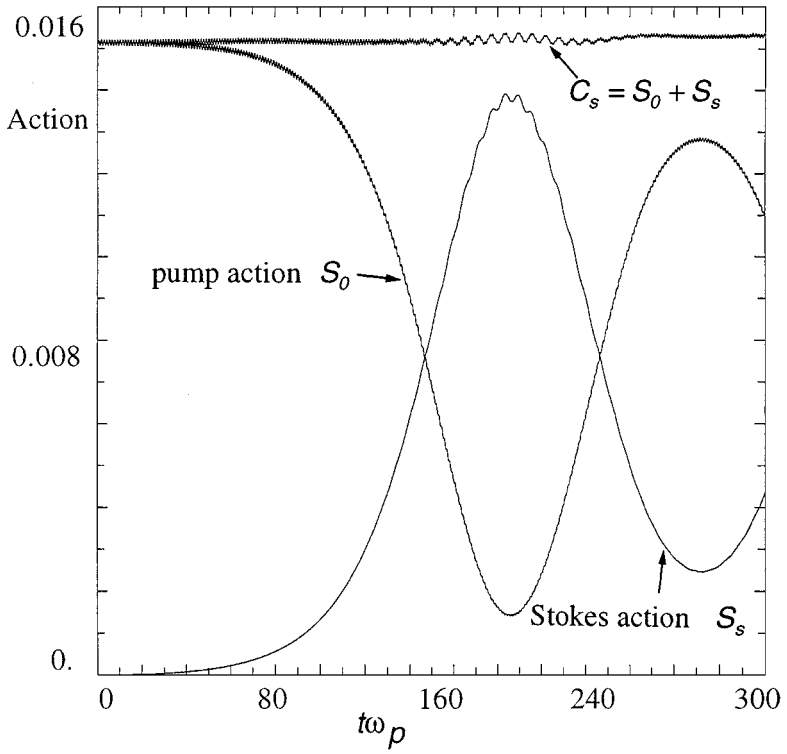

FIG. 1. Time behavior of the electromagnetic action densities obtained from the 2D semi-Lagrangian Vlasov code: The pump $S_o = a_o a_o^*$, the Stokes $S_s = a_s a_s^*$, and their sum $C_o = S_o + S_s$.

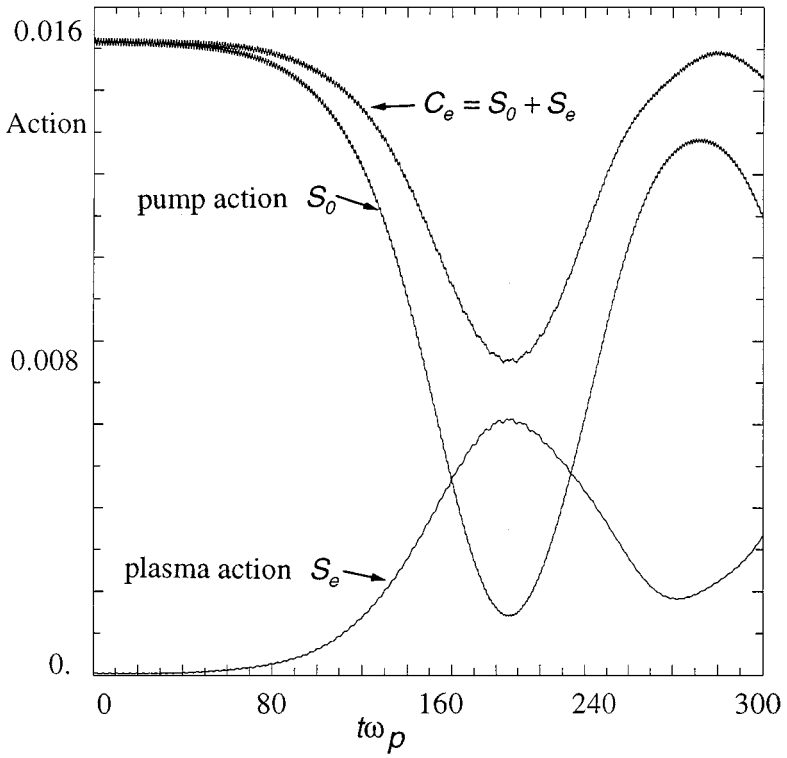

FIG. 2. Time behavior of the pump action density S_o and the plasma action density S_e and their action sum $C_e = S_o + S_e$ indicating the occurrence of action transfer from the plasma wave to accelerated particles.

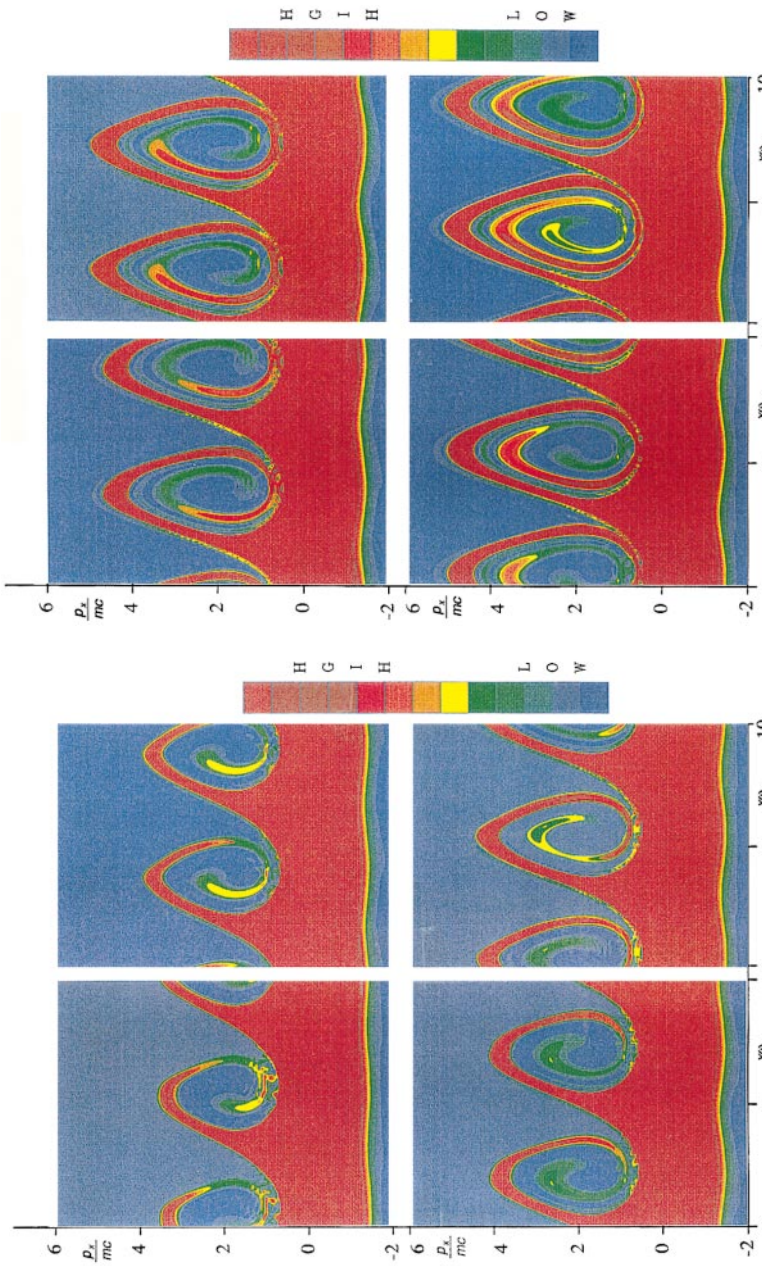

FIG. 3. The $x - p_x$ phase space representation afforded by the Vlasov code from time $t\omega_p = 130$ until $t\omega_p = 200$ by step of $10\omega_p^{-1}$. They clearly exhibit the acceleration of positive particles followed by trapping and the formation of vortices induced by FRS.

4.2. *Gaussian Pump Laser Profile*

To further illustrate the influence of transverse effects on the particle acceleration mechanism, a numerical simulation with a pump light with a gaussian amplitude profile is then investigated. The numerical resolution of Maxwell's equations (11) to (13) requires in that case the knowledge of the initial electromagnetic field B_x, B_y, and momemtum P_z for a gaussian profile amplitude of E_z given in the form $E_{zo}(y) = E_o e^{-\beta(y-y_o)^2}$. We choose $eE_o/m\omega_p c = 0.35$. Thus the fields are computed by considering an electromagnetic wave propagation in a homogeneous plasma. Assume an expression of the electric field in the following form, with $\zeta(t) = \omega(k_y)t - k_o x - k_y y$,

$$E_z(x, y, t) = \frac{1}{\sqrt{2\pi}} \int_{-\infty}^{+\infty} dk_y \tilde{E}_o(k_y) \exp i\zeta(t), \tag{24}$$

where $\tilde{E}_o(k_y)$ is the Fourier transform of the amplitude profile. Equations (11), (12), and (9) lead to the analytic solutions for B_x, B_y, P_z, at time $t\omega_p = -\Delta t/2$,

$$B_x(x, y, -\Delta t/2) = \frac{1}{\sqrt{2\pi}} \int_{-\infty}^{+\infty} dk_y \frac{k_y \tilde{E}_o}{\omega(k_y)} \exp i\zeta(-\Delta t/2) \tag{25}$$

$$B_y(x, y, -\Delta t/2) = \frac{1}{\sqrt{2\pi}} \int_{-\infty}^{+\infty} dk_y \frac{-k_o \tilde{E}_o}{\omega(k_y)} \exp i\zeta(-\Delta t/2) \tag{26}$$

$$P_z(x, y, -\Delta t/2) = \frac{1}{\sqrt{2\pi}} \int_{-\infty}^{+\infty} dk_y \frac{-ie\tilde{E}_o}{\omega(k_y)} \exp i\zeta(-\Delta t/2), \tag{27}$$

where the electromagnetic frequency $\omega = \omega(k_y)$ obeys the dispersion relation

$$\omega^2 = \omega_p^2 + k_o^2 c^2 + k_y^2 c^2 = \omega_o^2 + k_y^2 c^2. \tag{28}$$

This second numerical simulation is conducted with a maximum quiver velocity of $p_{osc}/mc \sim 0.134$ located initially at $y = L_y/2$. The time step used here is $\Delta t\omega_p = 0.05$. Using a phase space grid of $N_x N_y N_{p_x} N_{p_y}$ of $64 \times 32 \times 128 \times 32$, i.e., 8,388,608 "particles," the CPU time on the Cray-C94 computer is 0.56 μs per time step per grid point, i.e., about 8 h CPU time up to 300 ω_p^{-1}. Detailed comparison of the code version on the parallel T3D-T3E computer will be given later. The corresponding phase space plots of the distribution function $f(x, y = L_y/2, p_x, p_y = 0)$ are shown in Fig. 4. Similar particle acceleration structures can be seen with spirals inside the vortex structure which implicitly reflect the history of the particles trapped as the wave built up. There are, however, little changes in maximum momentum leading to an acceleration until $mc^2(\gamma - 1) \sim 1.5$ MeV.

5. NUMERICAL SIMULATION OF CASCADE PROCESSES

Among the studies that have been undertaken to discover new techniques to accelerate particles up to ultrarelativistic energies, the ones based on the generation of large amplitude plasma waves (theoretically capable of reaching an electric field of the order of GeV/m) seem very promising. A second way to obtain an electric field of such intensity is to inject two electromagnetic waves in plasma of low density (laser beatwave concept). To obtain fields as strong as possible, the difference of frequencies of the two waves must be chosen to

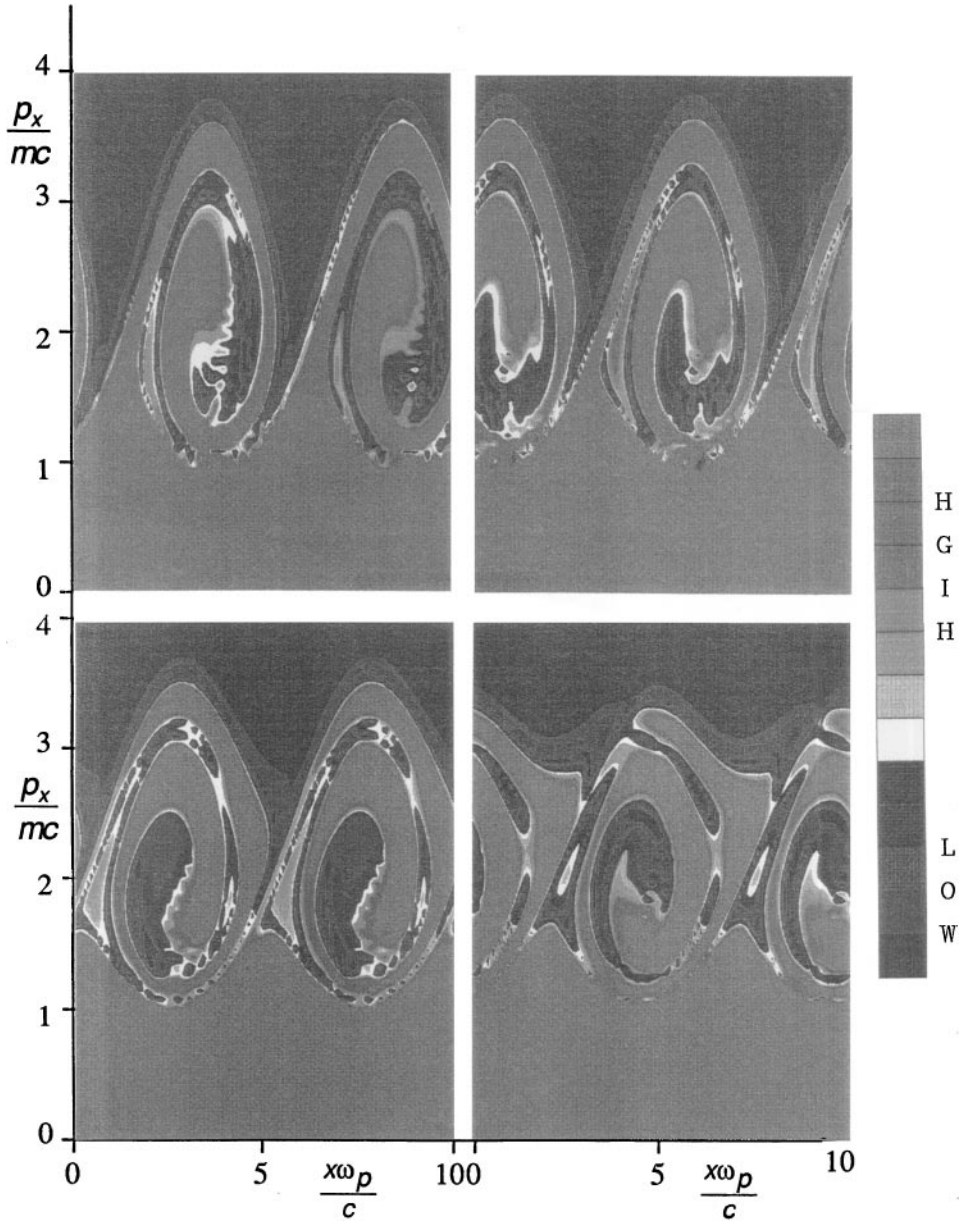

FIG. 4. The $x - p_x$ phase space representation in the case of a transverse gaussian profile of the laser light at different times during plasma evolution $t\omega_p = 140, 160, 180, 200$.

resonate with the plasma frequency. In these conditions the beat of these two electromagnetic waves induces by resonance a high-phase velocity longitudinal wave, which traps and accelerates electrons to ultrarelativistic energies. The recent UCLA (University of California at Los Angeles) experiment ratio of pump frequency to plasma frequency is very high ($\omega_{pump}/\omega_{plasma} \approx 33$), which makes it difficult to describe such experiments by numerical simulations with the usual numerical codes. Because this high ratio imposes a prohibitive computer burden on a direct attack via Eulerian Vlasov or particle-in-cell (PIC) simulation, we have recently proposed a hybrid model: the one-and-one-half dimension ($1\frac{1}{2}D$) Eulerian

Vlasov code (see Refs. [11, 12]) which has been modified to interface with the high-frequency complex envelopes rather than interfacing directly with the elctromagnetic part of the Maxwell equations. The important physics are taking place on the plasma period time scale; the light waves that are generating the plasma wave have frequencies of 30 or more times the plasma frequency (see Refs. [9, 10]). The hybrid model (which we have called the Hilbert–Vlasov code, HV) becomes an efficient method to investigate in detail the physics of beatwave experiments and we expect that the HV code is doing a good job of imitating the full electromagnetic Maxwell–Vlasov code at 1/1000 of the cost.

However, in beatwave experiments, self focusing, side scattering, cascade processes are also important. Therefore a two-dimensional model is required. For economy in the analysis of our problem, our pump frequency is chosen to be smaller than the experiment and in order to take into account all electromagnetic effects induced by side scattering and the cascade mechanism of the electromagnetic waves, a Vlasov–Maxwell model is used here.

In this section we present results from a 2D Vlasov simulation to investigate the relative importance of Raman scattering (forward scattering, side scattering) and cascade focusing. The cascade process is a more complicated situation in which, if a sufficiently intense Stokes (or idler here) wave is generated, it can then act as a secondary pump wave and generate a higher-order Stokes shifted wave at frequency $\omega_{2s} = \omega_s - \omega_e$ and so on. A whole hierarchy of higher order Stokes/anti-Stokes sidebands can be generated in this fashion (however, the anti-Stokes wave is in this case attenuated rather than amplified). By choosing a high pump frequency value ($\omega_o = 4.147\omega_p$), it is then possible to excite a cascade process, but also a side scattering process in beatwave excitation provided that the length box L_y is sufficient. The choice of a pump wavenumber of $k_o c/\omega_p = 7\Delta k \simeq 4.025$ (where $\Delta k = 2\pi/L_x = 0.575\omega_p/c$ is the fundamental wavenumber in the x direction) allows a rich variety of possible coupling (Raman cascades and side scattering and its cascade). The corresponding idler wave is $\omega_s = 3.043\omega_p$.

A first series of simulations is performed to illustrate an example of down-cascading of the idler wave to a second Stokes component in the case of a beatwave experiment. The frequency spectrum of the transverse electromagnetic field E_z is presented in Fig. 5. Idler and pump peaks are clearly resolved in the electromagnetic spectrum and the peaks are in good agreement with the predictions obtained from the matching conditions and linear dispersion relations (see Table I). As expected, the second Stokes ($\omega_{2s} = 1.993\omega_p$) can be seen in the electromagnetic spectrum (this electromagnetic spectrum exhibits an anti-Stokes component close to the theoretical value $\omega_{as} = 5.270\omega_p$ but also a third Stokes and second anti-Stokes cascade frequency close to $\omega_{3s} \sim \omega_p$ and $\omega_{2as} \simeq 6.3\omega_p$, but these components remain at a very small level). Looking at the electromagnetic action density evolution gives a more precise comparison between both modes. The longitudinal action densities $S_o = a_o a_o^*(k_x = k_o, k_y = 0)$ (for pump), S_s (for idler), S_{2s} (for the one-step cascade Stokes), S_{3s} (for the second step cascade Stokes), S_{as} (for the anti-Stokes) together with their sum C_s are shown in Fig. 6 (which is the first electromagnetic Manley–Rowe invariant). As expected the action sum C_s is well conserved (to within 3%).

The semi-Lagrangian Vlasov code allows thus a precise comparison with the mode coupling theory and with the Manley–Rowe invariants. But the most striking advantage of this model is the very fine resolution in phase space capable to resolving the finest mechanism

TABLE I

Pump wave	Scattered wave	Plasma wave	$\Delta\omega$
$\vec{k}_o(7\Delta k, 0)$ $\omega_o = 4.147\omega_p$	$\vec{k}_s(5\Delta k, 0)$ $\omega_s = 3.043\omega_p$	$\vec{k}_e(2\Delta k, 0)$ $\omega_e = 1.056\omega_p$	$0.046\omega_p$
$\vec{k}_s(5\Delta k, 0)$ $\omega_s = 3.043\omega_p$	$\vec{k}_{2s}(3\Delta k, 0)$ $\omega_s = 1.993\omega_p$	$\vec{k}_e(2\Delta k, 0)$ $\omega_e = 1.056\omega_p$	$-0.006\omega_p$
$\vec{k}_{2s}(3\Delta k, 0)$ $\omega_s = 1.993\omega_p$	$\vec{k}_{3s}(\Delta k, 0)$ $\omega_s = 1.153\omega_p$	$\vec{k}_e(2\Delta k, 0)$ $\omega_e = 1.056\omega_p$	$-0.21\omega_p$
$\vec{k}_{as}(9\Delta k, 0)$ $\omega_{as} = 5.270\omega_p$	$\vec{k}_o(7\Delta k, 0)$ $\omega_o = 4.147\omega_p$	$\vec{k}_e(2\Delta k, 0)$ $\omega_e = 1.056\omega_p$	$-0.06\omega_p$
$\vec{k}_o(7\Delta k, 0)$ $\omega_o = 4.147\omega_p$	$\vec{k}_s(5\Delta k, \pm\Delta k)$ $\omega'_s = 3.097\omega_p$	$\vec{k}_e(2\Delta k, \pm\Delta k)$ $\omega'_e = 1.070\omega_p$	$-0.02\omega_p$
$\vec{k}'_s(5\Delta k, \pm\Delta k)$ $\omega'_s = 3.097\omega_p$	$\vec{k}'_{2s}(3\Delta k, \pm\Delta k)$ $\omega'_{2s} = 2.075\omega_p$	$\vec{k}'_e(2\Delta k, \pm\Delta k)$ $\omega'_e = 1.070\omega_p$	$-0.10\omega_p$
$\vec{k}'_{as}(9\Delta k, \pm\Delta k)$ $\omega'_s = 5.125\omega_p$	$\vec{k}_o(7\Delta k, 0)$ $\omega_o = 4.147\omega_p$	$\vec{k}'_e(2\Delta k, \pm\Delta k)$ $\omega'_e = 1.070\omega_p$	$-0.09\omega_p$

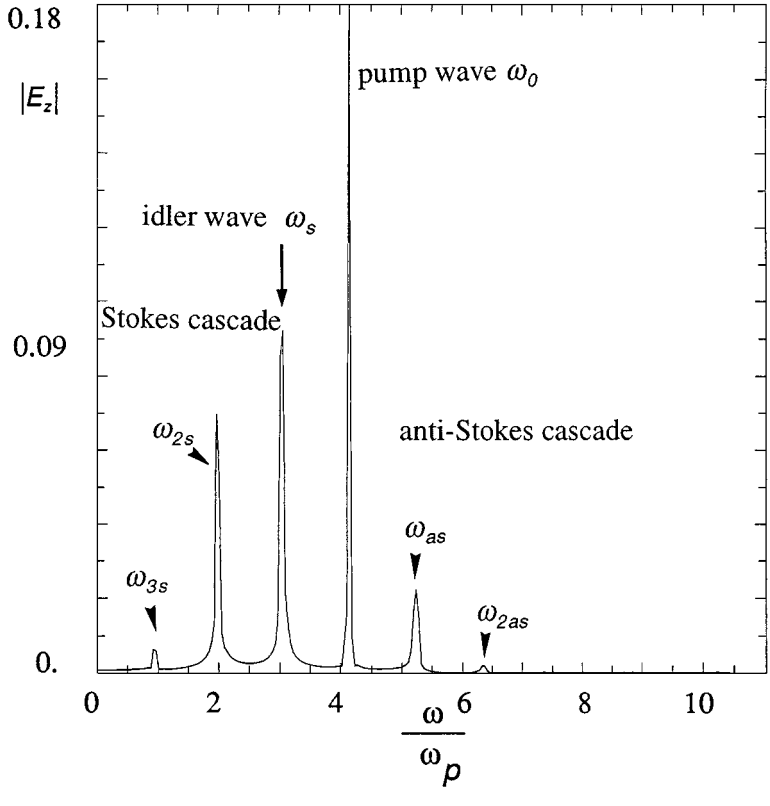

FIG. 5. Frequency spectrum of the transverse electromagnetic field E_z: idler and pump peaks are in good agreement with the theoretical values $\omega_s = 3.043\omega_p$ and $\omega_o = 4.147\omega_p$. The electromagnetic spectrum exhibits also down-shifted (Stokes) and up-shifted (anti-stokes) peaks due to cascade processes.

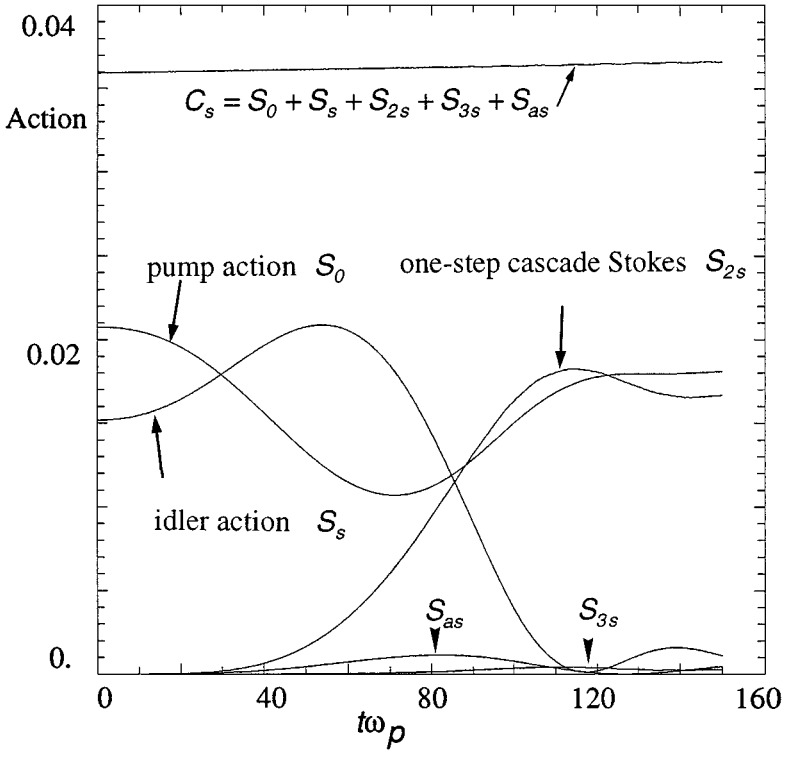

FIG. 6. Electromagnetic action density evolution of pump (S_0), idler (S_s), one-step cascade Stokes (S_{2s}), second-step cascade Stokes (S_{3s}), and anti-Stokes (S_{as}) together with their mutual sum C_s (corresponding to the first electromagnetic Manley–Rowe invariant), obtained in the case of an homogeneous transverse laser profile.

of particle acceleration. In Fig. 7 the plots of the distribution function $f(x=0, y=L_y/2, p_x, p_y)$ are presented at various times showing the formation of an accelerated particle beam without transverse dispersion. More details of particle acceleration can be found in Fig. 8 in which we have represented the time evolution of the distribution function $f(x, y=L_y/2, p_x, p_y=0)$ in the $x-p_x$ phase space plane. Figure 8 exhibits clearly again the acceleration of positive velocity particles followed by trapping and the formation of vortices around a momentum corresponding to the plasma wave velocity $v_\varphi/c \simeq 0.918$ or $p_\varphi/mc \simeq 2.32$.

With minor modifications, the 2D Vlasov code can also simulate the Raman side scattering processes. By modifying the initial distribution perturbation in order to allow the growth of this instability (we just perturb now the corresponding plasma mode in density with an amplitude of 10^{-2}), a second series of numerical simulations is carried out to analyze the influence of two-dimensional effects. The frequency spectra of the transverse electromagnetic fields B_x and B_y are illustrated respectively in Figs. 9 and 10. The peaks of the B_y-part of the electromagnetic wave correspond to the classical cascade process met previously by the idler wave and its decay. The dominant peaks in the B_y spectrum correspond to the pump and idler wave, and the values obtained here match rather well with the theoretical values. On the other hand, the growth of the x-component of the magnetic field cannot be interpreted without taking into account now two-dimensional effects such as side scattering because this component cannot be excited in a purely one-dimensional model. The B_x magnetic spectrum exhibits the growth of a cascade process of the side

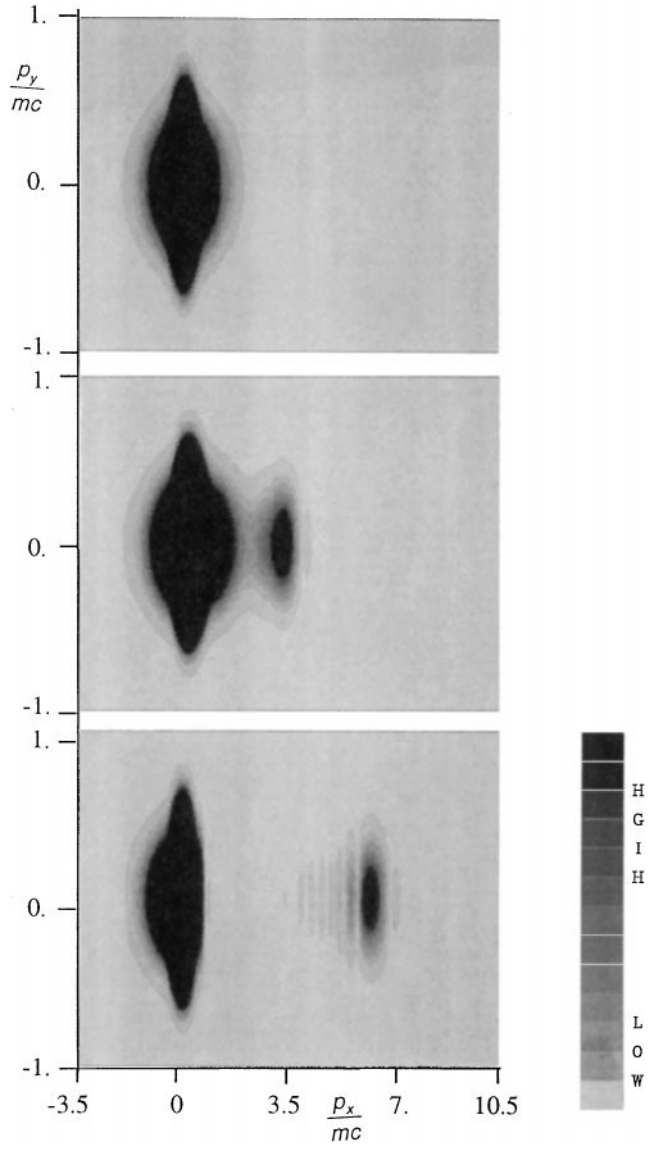

FIG. 7. Distribution function plots $f(x=0,\, y=Ly/2,\, p_x,\, p_y)$ at times $t\omega_p = 8,\, 98,\, 143$, during plasma evolution showing the formation of an accelerated particle beam without transverse dispersion.

scattering mode with dominant peaks located at $\omega_1 \sim 2\omega_p$ and $\omega_2 \sim 3\omega_p$. Further confirmation of the occurring of side scattering is provided in the examination of the action density evolution. In Fig. 11 we have again plotted the time evolution of S_o, S_s, S_{2s}, S_{3s}, S_{as}, and their sum C_s (the different actions are computed using a two-dimensional Fourier transform and then selecting the corresponding modes $k_x = k_o, k_s, k_{2s}$, and so on, with $k_y = 0$). Now C_s exhibits a strong decrease which seems to indicate that the plasma evolves in a more complicated way leading to the excitation of transverse electromagnetic modes. Figure 12 show the plots of $f(x=0, y=L_y/2,\, p_x,\, p_y)$. In spite of choosing a particular position in the configuration space, the behavior of the distribution function remains similar at another point of the configuration space. The different plasma waves generated as a result of Raman

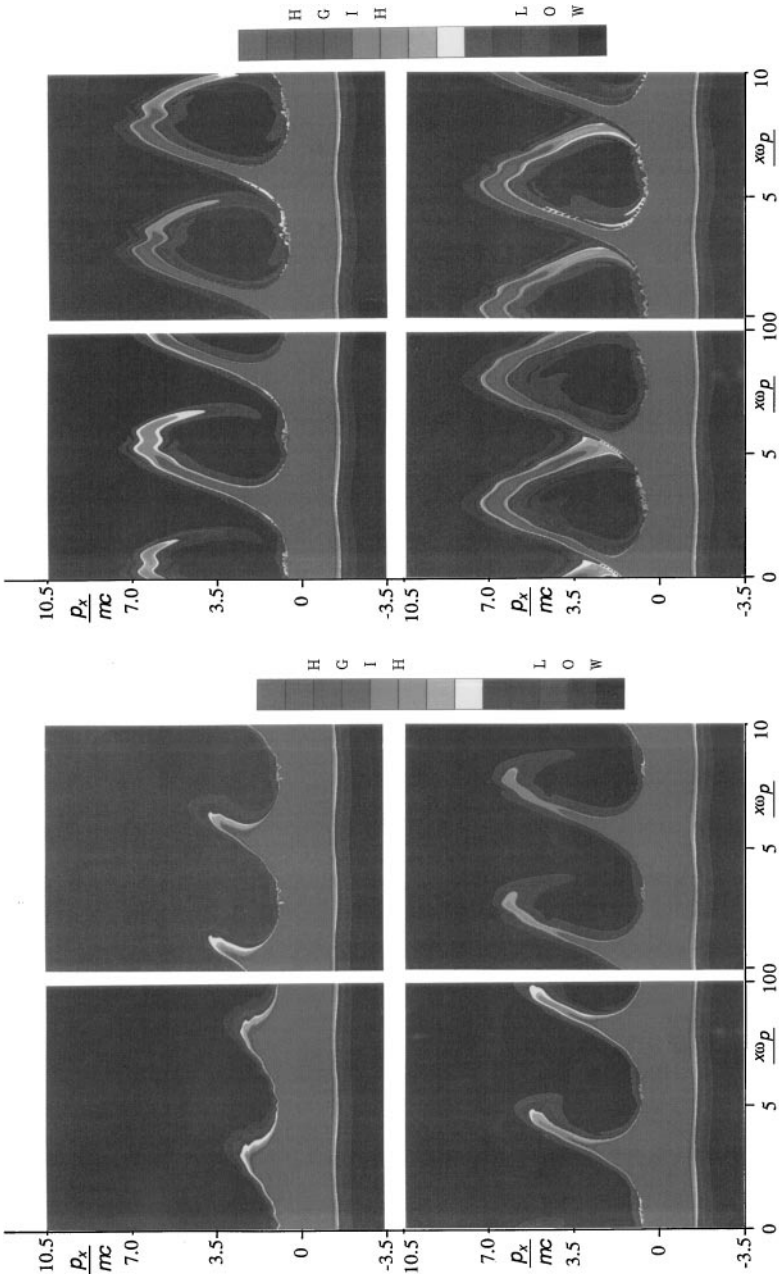

FIG. 8. Detailed examination of the acceleration mechanism directly in the $x - p_x$ phase space. We have plotted the distribution function located at $y = L_y/2$ and $p_y = 0$ at different times during plasma evolution.

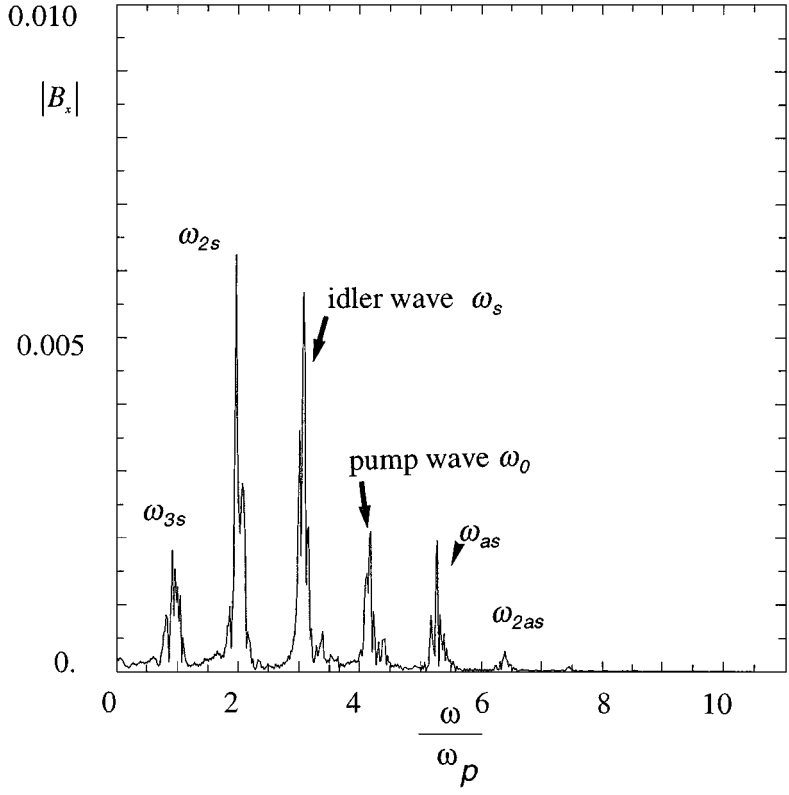

FIG. 9. Frequency spectrum of the B_x magnetic field component showing the occurring of side scattering and side cascade processes in plasma.

side scattering coupling can give rise to a strong plasma turbulence, which is responsible for longitudinal electron acceleration and also a strong "heating" or stochastic acceleration in the perpendicular direction (y-axis).

6. OPTIMIZATION AND PERFORMANCE

All present results were processed on the Cray C94-C98, Cray T3D, and Cray T3E computing systems. The vectorized version of the Vlasov code achieved a data processing rate of 250 Mflops and demonstrated a reasonably high vectorized efficiency. Two grid system $N_x N_y N_{p_x} N_{p_y}$ of $128 \times 8 \times 128 \times 32$ and then of $128 \times 32 \times 128 \times 32$ were investigated resulting in a corresponding number of 4,194,306 and 16,777,216 particles. The CPU time was close to 0.54 μs per time step per particle on the Cray C94 computer while a first version of the parallelized code gave a value of 24, 64 μs per time step per particle and per processor.

The primary task of converting a code to run on a distributed memory machine is to optimize array layouts in memory so that the computational load is well balanced among the processors. In our simulation model, the distribution function is partitioned into blocks and this methodology simplifies the programming structure and loads to natural load-balancing of all the processors. Cubic spline interpolation introduced at each step of the splitting scheme requires tridiagonal matrix inversions. One method for parallelizing matrix operations is

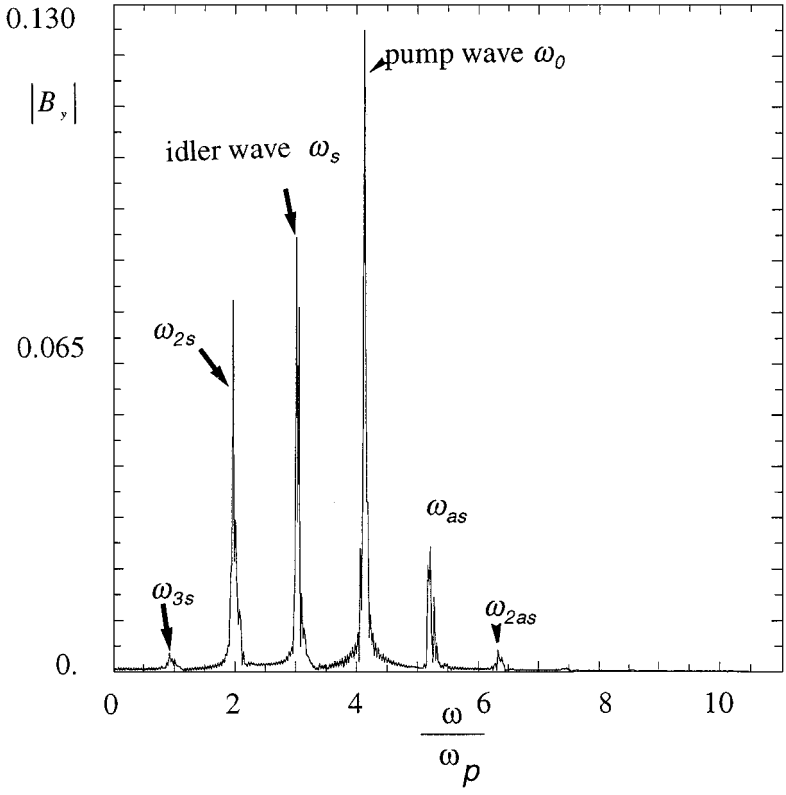

FIG. 10. Frequency spectrum of the B_y magnetic field component with the usual dominant peaks characterizing the pump and idler longitudinal cascade.

to split the matrix into submatrices and follow a fork-and-join model (with local cyclic reduction algorithm; see for instance Refs. [13, 14]), where each processor is given some number of operations to perform local factorization of partitioned matrices). For the present simulations, a much simpler approach, i.e., static domain decomposition followed by matrix transposition, was chosen. For example, in order to compute the matrix inversion along the x direction, the domain was partitioned into the p_x-direction and then a transposition was necessary to inverse the tridiagonal matrix along the p_x-direction.

A substantial amount of improvement was achieved by optimizing the node-to-memory communications which critically affect the parallel efficiency. The optimized version led then to a CPU time of 9.5 μs per time step, per particle, per processor. The numerical efficiency improvement was by a factor of 3 and seemed to indicate that one processor of the Cray C94 is equivalent to 20 processors on the T3D computer (and equivalent to 18 processors on the T3E computer). For example, the last simulation presented in this section was carried out using a grid sampling $N_x N_y N_{px} N_{py}$ of $128 \times 32 \times 256 \times 32$, i.e., 33,554,432 particles and took 7 h on the T3E computer using 32 processors for 3000 time steps, i.e., 8.03 μs per time step, per particle, per processor.

For this simulation the load balance measured by considering the total CPU time (communication plus calculation) divided by the number of processors and by the total elapsed time led to a value of 0.94. (If all of the processors are busy all of the time, then the above ratio will be unity.) The ratio for the 2D Vlasov code of 0.94 indicated a reasonably

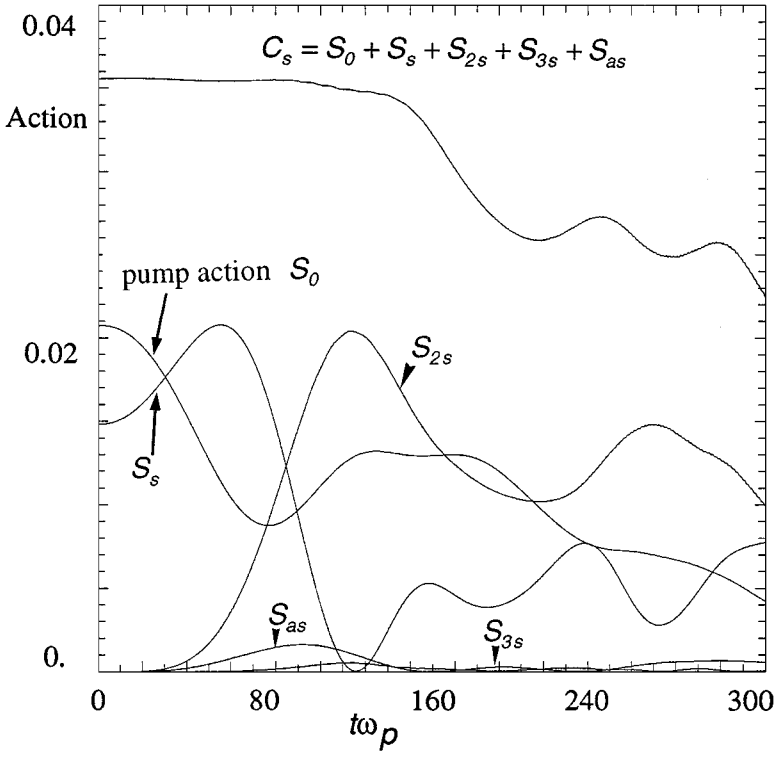

FIG. 11. Time evolution of the corresponding electromagnetic action density S_o (pump wave), S_s (idler wave), S_{2s} (one-step longitudinal Stokes), $S_{2s} = a_{2s}a^*_{2s}(k_x = k_{2s}, k_y = 0)$, S_{3s} (second-step longitudinal Stokes), S_{as} (anti-Stokes wave), and their mutual sum C_s. Now C_s exhibits a strong decrease showing the excitation of transverse electromagnetic modes (due to side scattering).

efficient use of all processors. The efficient use of the processors was aided by choosing grid dimensions which matched the number of processors in a partition. If the code is run on a 64-node partition, then a grid resolution (on the x or p_x direction) of at least 64 points, or some multiple (we use 256 points) thereof, in at least one direction is optimal. The communication time required for the matrix transposition was close to 12% of the total CPU time in that case. Another measure of parallel efficiency is scalability, i.e., the reduction in computing time achieved when the number of processors is doubled. For the present code, wall clock times on the T3D computer were measured on the partition $N_x N_y N_{px} N_{py}$ of $256 \times 8 \times 256 \times 32$ to obtain the following measure of scalability,

$$T_{CPU\,16\text{-}node} / T_{CPU\,32\text{-}node} \simeq 2.108 \tag{29}$$

$$T_{CPU\,32\text{-}node} / T_{CPU\,64\text{-}node} \simeq 2.060. \tag{30}$$

Additional efficiency improvement for the present code is still possible by replacing global synchronous message passing calls with several asynchronous calls using the MPI[2] library or the non-standard SHMEM[3] library of the Cray system. In essence a sustained effort must be maintained to realized the full potential of scalable parallel systems.

[2] M.P.I., *m*essage *p*assing *i*nterface.

[3] SHMEM, *sh*ared *mem*ory.

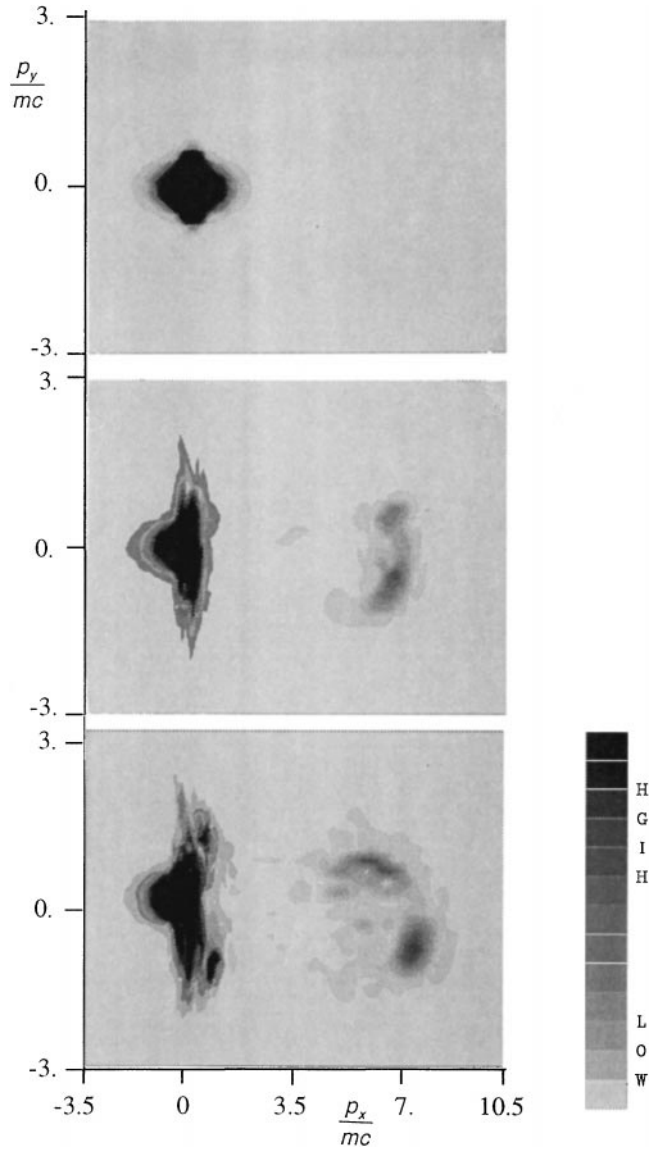

FIG. 12. Plots of the electron distribution function in the $p_x - p_y$ momentum space at $x = 0$ and $y = L_y/2$, at times $t\omega_p = 8$, 120, and 150, leading to a strong longitudinal electron acceleration and heating in the transverse spatial direction.

7. CONCLUSION

In order to investigate the transverse geometrical effects on the particle acceleration, numerical simulations using a two-dimensional relativistic and semi-Lagrangian Vlasov code have been carried out in an electromagnetic regime related to PBWA ad FRS. Due to the extremely large computational resources required for treating the distribution function described in a four variable phase space the use of a massively parallel computer was necessary and enabling. A Vlasov algorithm using a splitting scheme for message passing in a multi-computer environment was developed and implemented on T3D and T3E computers. Because of the Eulerian characteristic of the distribution function, the (semi-Lagrangian)

Vlasov code simplifies programming structure because one does not have to cope with the allocation of the particles between processors since Euler elements stay in place. This code employed a classic time splitting scheme, cubic spline interpolation, and matrix transposition and was adapted to optimally use the particular parallel architecture of the Cray T3D and T3E (both processor's specifications and node-to-node communications). The 2D Vlasov code gives a good description of the electron acceleration dynamics even in very low level regions of phase space. Both approaches (particles-in-cell and the Vlasov code) require a more complicated comparison of the interplay between the physics aspect of the model on the one hand and performance and optimization issues on the other. Future work will address the use of a full relativistic Vlasov model for the study of the laser wakefield at ultrahigh intensity.

ACKNOWLEDGMENTS

We thank E. Fijalkow for helpful comments and suggestions. The authors are indebted to the I.D.R.I.S. center (Institut du Développement et des Ressources en Informatique Scientifique- Paris France) for time allocation on the Cray C98-C94 and parallel Cray T3D-T3E computers.

REFERENCES

1. T. Tajima and J. M. Dawson, Laser electron accelerator, *Phys. Rev. Lett.* **43**, 267 (1979).
2. A. Ghizzo, P. Bertrand, M. Shoucri, T. W. Johnston, E. Fijalkow, and M. R. Feix, A Vlasov code for the numerical simulation of stimulated Raman scattering, *J. Comput. Phys.* **90**(2), 431 (1990).
3. T. W. Johnston, P. Bertrand, A. Ghizzo, M. Shoucri, E. Fijalkow, and M. R. Feix, Stimulated Raman scattering: Action evolution and particle trapping via Euler–Vlasov fluid simulation, *Phys. Fluids B* **4**(8), 2523 (1992).
4. P. Bertrand, A. Ghizzo, T. W. Johnston, M. Shoucri, E. Fijalkow, and M. R. Feix, A non-periodic Euler–Vlasov code for the numerical simulation of laser-plasma beat wave acceleration and Raman scattering, *Phys. Fluids B* **2**(5), 1028 (1990).
5. P. Bertrand, A. Ghizzo, S. J. Karttunen, T. J. H. Pättikangas, R. R. E. Salomaa, and M. Shoucri, Generation of ultrafast electrons by simultaneous stimulated Raman backward and forward scattering, *Phys. Rev. E* **49**(5), 5656 (1994).
6. A. Staniforth and J. Coté, Semi-lagrangian integration scheme for atmospheric models, a review, *Monthly Weather Rev.* **119**, 2206 (1991).
7. C. G. Cheng and G. Knorr, The integration of the Vlasov equation in configuration space, *J. Comput. Phys*. **22**, 330 (1976).
8. M. Shoucri, Numerical solution of the two-dimensional Vlasov equation, *IEEE Trans. Plasma Sci*. **7**(2), 69 (1979).
9. C. E. Clayton, K. A. Marsh, A. Dyson, M. Everett, A. Lal, W. P. Leemans, R. Williams, and C. Joshi, Ultrahigh-gradient acceleration of injected electrons by laser-excited relativistic electron plasma waves, *Phys. Rev. Lett*. **70**(1), (1993).
10. C. E. Clayton, M. Everett, A. Lal, D. Gordon, K. A. Marsh, and C. Joshi, Acceleration and scattering of injected electrons in plasma beat wave accelerator experiments, *Phys. Plasmas* **1**(5), (1994).
11. A. Ghizzo, P. Bertrand, J. Lebas, T. W. Johnston, and M. Shoucri, A hybrid eulerian Vlasov code. I. Study of high-frequency beatwave experiment and Manley–Rowe action evolution in a finite causal system, *Phys. Plasma* **3**(2), 650 (1996).
12. A. Ghizzo, P. Bertrand, M. L. Bégué, T. W. Johnston, and M. Shoucri, A Hilbert–Vlasov code for the study of high-frequency Plasma Beatwave Accelerator, *IEEE Trans. Plasma Sci*. **24**(2), 370 (1996).
13. L. Brugnano, A parallel solver for tridiagonal linear systems for distributed memory parallel computer, *Parallel Comput*. **17**, 1017 (1991).
14. P. Amodio, L. Brugnano, and T. Politi, Parallel factorizations for tridiagonal matrices, *Parallel Comput*. **5**, 813 (1992).